



Seismic anisotropy beneath Cascadia and the Mendocino triple junction: Interaction of the subducting slab with mantle flow

Caroline M. Eakin^{a,b,*}, Mathias Obrebski^a, Richard M. Allen^a, Devin C. Boyarko^c, Michael R. Brudzinski^c, Robert Porritt^a

^a Department of Earth and Planetary Sciences, University of California, 307 McCone Hall, Berkeley, CA 94720, USA

^b Department of Earth Science and Engineering, Imperial College London, UK

^c Department of Geology, Miami University, Oxford, Ohio 45046, USA

ARTICLE INFO

Article history:

Received 10 September 2009

Received in revised form 30 June 2010

Accepted 7 July 2010

Available online 3 August 2010

Editor: R.D. van der Hilst

Keywords:

Cascadia subduction

Mendocino Triple Junction

Gorda-Juan de Fuca plate

slab edge

shear wave splitting

ABSTRACT

Mantle flow associated with the Cascadia subduction zone and the Mendocino Triple Junction is poorly characterized due to a lack of shear wave splitting studies compared to other subduction zones. To fill this gap data was obtained from the Mendocino and FACES seismic networks that cover the region with dense station spacing. Over a period of 11–18 months, 50 suitable events were identified from which shear wave splitting parameters were calculated. Here we present stacked splitting results at 63 of the stations. The splitting pattern is uniform trench normal (N67°E) throughout Cascadia with an average delay time of 1.25 s. This is consistent with subduction and our preferred interpretation is entrained mantle flow beneath the slab. The observed pattern and interpretation have implications for mantle dynamics that are unique to Cascadia compared to other subduction zones worldwide. The uniform splitting pattern seen throughout Cascadia ends at the triple junction where the fast directions rotate almost 90°. Immediately south of the triple junction the fast direction rotates from NW–SE near the coast to NE–SW in northeastern California. This rotation beneath northern California is consistent with flow around the southern edge of the subducting Gorda slab.

© 2010 Elsevier B.V. All rights reserved.

1. Introduction

The Mendocino Triple Junction (MTJ) is located on the coast of northern California and marks the intersection of the North American, Pacific and Gorda-Juan de Fuca (G-JdF) plates (see Fig. 1). To the north is the Cascadia subduction zone where the Juan de Fuca plate, a fragment of the ancient Farallon plate, is subducting beneath North America. To the south and west are the San Andreas and Mendocino transform faults respectively.

The subducting G-JdF slab is young (7–10 Ma) and therefore thin (<50 km) due to the proximity of the ridge to the west (Severinghaus and Atwater, 1990; Wilson, 1993). The slab has been previously imaged to a depth of 400 km in the southern section of the subduction zone with an approximate dip of 50° towards the east (Xue and Allen, 2007). The slab is undergoing rollback, i.e. the trench is moving progressively towards the oceanic plate (Zandt and Humphreys, 2008). North America has an absolute motion of 27 mm/yr towards the southwest (Gripp and Gordon, 2002) and is therefore overriding the G-JdF plate at a faster rate than the oceanic plate subducts.

Although the tectonic history of the region is well characterized from plate reconstructions and tomography, how the subduction has affected mantle flow is relatively unknown. Such knowledge about the mantle flow field is primarily obtained from studies of mantle anisotropy using observations such as shear wave splitting. There has been much attention given to other subduction zones including Japan where there have been numerous shear wave splitting studies (Ando et al., 1983; Fouch and Fischer, 1996; Long and van der Hilst, 2005; Nakajima and Hasegawa, 2004; Sandvol and Ni, 1997; Tono et al., 2009, etc.). In contrast Cascadia is lacking in such measurements, yet has shown patterns that are unique to the global data set, i.e. trench perpendicular fast directions beneath the slab, for which there is no obvious explanation as to why Cascadia is the exception (Long and Silver, 2008; Long and Silver, 2009). Work by Currie et al. (2004) is the most extensive to date, focusing on northern Cascadia around the US–Canada border. In addition there have been some other previous studies within Cascadia looking at a small number of stations (Bostock and Cassidy, 1995; Fabritius, 1995; Hartog and Schwartz, 2000; Polet and Kanamori, 2002; Xue and Allen, 2006) all of which have limited spatial coverage. As a result there is currently an absence of splitting measurements covering the Pacific Northwest.

The Mendocino Triple Junction is also an important tectonic feature of the region. Until now there have been limited splitting observations close to the triple junction, despite a pronounced change in the orientation of the splitting measurements at this location and also the transition across

* Corresponding author. Department of Earth and Planetary Sciences, University of California, 307 McCone Hall, Berkeley, CA 94720, USA. Tel.: +1 510 642 1275; fax: +1 510 643 5811.

E-mail address: eakin@seismo.berkeley.edu (C.M. Eakin).

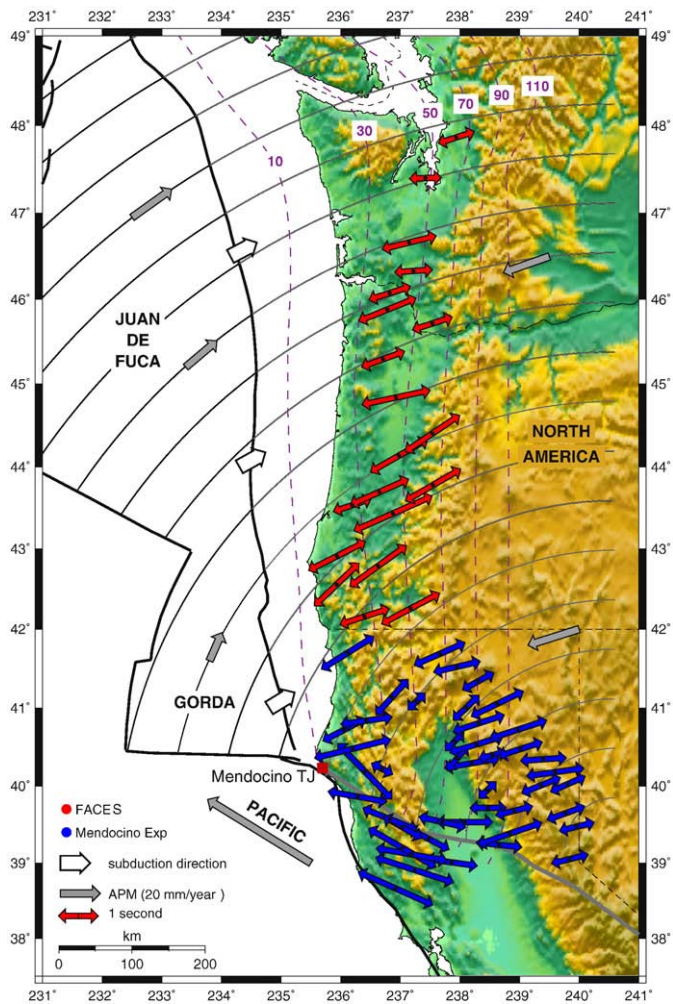


Fig. 1. Tectonic map for the study region including stacked shear wave splitting results. The blue (FACES experiment) and red (Mendocino experiment) arrows are orientated according to the fast direction calculated for that station, and their length is proportional to the delay time. The fast direction is uniform (average: N67°E) throughout much of Cascadia. However there is a marked contrast across the southern edge of the G-JdF slab (thick grey line). Light grey arrows represent the absolute plate motion (Gripp and Gordon, 2002). Thin black lines (motion vectors) have been drawn to emphasize the rotational movement of the G-JdF plate as determined from its absolute plate motion. White arrows show the subduction direction i.e. the relative plate motion between G-JdF plate and North American plate. Thick black lines are plate boundaries. The southern edge of the G-JdF slab was determined by mapping out the southern end of the high velocity slab anomaly imaged in the DNA09-P velocity model (Obrebski et al., in press). Estimated depths of the top of the subducting slab are drawn as dashed purple lines.

the edge of the underlying G-JdF slab. Both of these factors are important to recent discussions in the literature of the large-scale circular splitting pattern (the 'Nevada swirl') observed across the western US (Zandt and Humphreys, 2008; West et al., 2009).

Here we present shear wave splitting observations made using the data sets from two of Earthscope's Flexible Array deployments in the Pacific Northwest. The splitting observations are consistent with previous studies but provide a much higher density of measurements allowing us to better constrain possible mantle flow geometries.

2. Shear wave splitting

This study makes use of shear wave splitting which is based upon the principle that as a shear wave passes through an anisotropic material it is split into 2 perpendicular components polarized in a fast

and slow direction. The two components have different velocities and accumulate a delay time (δt) between them as they travel through an anisotropic medium. SKS and SKKS phases are most often used in shear wave splitting studies. Such phases are polarized into a single direction (the radial plane) after traveling through the core as a P wave. The splitting measurements are thus simplified and any effect of source side anisotropy is removed.

The main source region of anisotropy is thought to be in the upper mantle (Gaherty and Jordan, 1995), specifically from the lattice preferred orientation (LPO) of olivine (the most abundant anisotropic mineral). The a-axis of Olivine has been shown to align parallel with the direction of strain (Zhang and Karato, 1995). The fast direction can therefore be directly related to ongoing deformation and flow of the upper mantle. The lithosphere can also be a potential source of fossilized anisotropy but its effect is only relevant in regions where the lithosphere has a substantial thickness such as a continental craton (Silver and Chan, 1991). In the western US the lithosphere is too weak and thin (~70 km) for this to be the case (Li et al., 2007).

This study uses data from two seismic networks: the Mendocino experiment and FACES (Flexible Array Along Cascadia Experiment for Segmentation). The Mendocino experiment is a dense network of 74 seismic stations across Northern California with an average station spacing of 25 km (see Fig. 1 for station locations). The stations were installed in 2 main phases during July and October of 2007. FACES stations are all located in the forearc of the Cascadia subduction zone extending to the Mendocino network northwards along the coast of Oregon and Washington with an average spacing of 40 km. The 23 FACES stations were installed in November 2007 and most have real time telemetry using cellular phone modems. At the time of this study data was available over an 11 month period from October 2007 to September 2008 for Mendocino and for 18 months from November 2007 until July 2009 for FACES.

In total 50 suitable seismic events were identified, corresponding to over 1500 waveforms from which we analyzed the SKS and SKKS phases. A list of all the events used is given in Supplementary material. As with similar studies in the western US making use of temporary seismic networks (e.g. Long et al., 2009), the range of back azimuths is restricted, especially for Mendocino data where the available time period was shorter. The majority of events are located in one quadrant (210°–315°) and mostly originated in the Tonga and Indonesian subduction zones. Events of magnitude greater than 6.3 and in the epicentral distance range of 85° to 130° were selected. This prevented the SKS/SKKS arrivals from overlapping with any other shear wave phases, whilst ensuring that the arrivals still have enough energy (Silver and Chan, 1988).

Shear wave splitting analysis was performed using the SplitLab package (Wüstfeld et al., 2007). An example of a shear wave splitting calculation from SplitLab is given in Supplementary material. In each case a bandpass filter of 0.03 to 0.3 Hz was applied to reduce noise. Several time windows were tested to check the stability of the results and to choose the window that produced the best constrained values (i.e. with the narrowest error regions). The fast direction (Φ) and delay time (δt) are determined via a grid search within SplitLab using two different methods: minimum energy of Silver and Chan (1988, 1991) and rotation correlation of Bowmann and Ando (1987). Calculating splitting parameters via two different methods is helpful when assessing the reliability of the result, but the final Φ and δt presented in our results are that of the minimum energy method as it is more stable over a wider range of back azimuths (Wüstfeld and Bokelmann, 2007).

Each of the measurements for which a clear fast direction could be determined was classified as good, fair, or poor. During classification many different factors were taken into account. These include subjective measures such as whether the SKS phase displays a similar shape in the estimated fast and slow directions, whether the corrected SKS phase shows very little energy on the transverse component, and whether the originally elliptically polarized SKS waves have a linear polarization in the

back azimuth direction after correction (e.g. Barruol et al., 1997). Classification is also dependent on quantitative measures. The signal to noise ratio of the uncorrected transverse component was required to be greater than five and errors of less than 1 s for δt and 22.5° for Φ at the 95% confidence level were necessary (Xue and Allen, 2006). Finally, an agreement in the splitting parameters derived using the two approaches was preferred, i.e. the difference in fast direction should be less than 22.5° and the ratio of delay times should be greater than 0.7 (Wüstfeld and Bokelmann, 2007). When all these criteria were satisfied the split was rated as 'good', when many were satisfied it was rated as 'fair'. A 'poor' classification was given where the seismograms were noisier than usual ($\text{SNR}_T < 10$) or SKS energy was lower. On their own poor measurements cannot be relied upon but can complement the data set when they are consistent with better quality observations at the same or nearby stations. Finally the average splitting parameters for each station were determined by stacking all the error matrices that resulted from a grid search for the best estimates of Φ and δt for each SKS/SKKS observation, and taking the global minimum.

3. Results

Out of over 1500 waveforms analyzed a total of 218 splitting measurements were made on SKS and SKKS phases (a complete list is given in Supplementary material). Stacked results were possible at 63 stations and are shown in Fig. 1. The splitting pattern is highly uniform throughout the length of Cascadia (~1000 km) and also east–west across the subduction zone from the forearc into the backarc as seen from the results of the Mendocino network in northern California north of the MTJ. The mean fast direction over the subduction zone is $N67^\circ E$ with a standard deviation of 12° . Currie et al. (2004) obtained a very similar fast direction of $N70^\circ E$ in northern Cascadia. This direction is normal to the trench and is comparable to the absolute motion of North American plate ($N72^\circ E$), absolute motion of the G-JdF plate (as shown by motion vectors on Fig. 1), and also the subduction direction ($\sim N60^\circ E$) i.e. G-JdF relative to North America (Gripp and Gordon, 2002). The average delay time is 1.25 s. The splitting times in Oregon, especially in the southern half, are larger (average: 1.57 s) compared to further north in Washington and to the south in northern California (both around 1.1 s).

On the west coast at the latitude of the MTJ, the observed fast direction dramatically rotates. Fast directions to the south of the MTJ are almost perpendicular to those to the north. The distance separating stations ME35 and ME39 at which the change-over is observed is less than 40 km. The mean splitting direction for stations south of the MTJ is $N71^\circ W$ (standard deviation 12°) with an average splitting time of 1.48 s (0.3 s larger than the rest of the Mendocino network in northern California). There is also a gradual rotation from the NW–SE orientation immediately south of the triple junction back to a NE–SW orientation at stations to the east across the southern half of the Mendocino network (Fig. 1).

Fig. 2 shows our results, previous splitting observations in the region, and tomographically imaged upper mantle velocities. The splitting measurements encompass all published results to date for the region (Wang et al., 2008; Zandt and Humphreys, 2008; Long et al., 2009; West et al., 2009 and references therein). The tomography image is a vertical average of the velocity anomaly from the DNA09 P-wave model over the 100–400 km depth range (Obrebski et al., in press; <http://dna.berkeley.edu>) calculated over the depth range 100–400 km, the same depth range over which we might expect an anisotropic mantle (Hartog and Schwartz, 2000; Long and van der Hilst, 2005). It is worth noting that there is little change to the average velocity anomaly when we average from 100 km to only 200 or 300 km depth. The slab is represented by the north–south high velocity anomaly adjacent to the trench at a longitude of 239° . The rotation of the splits from a NW–SE orientation immediately south of the triple junction to a NE–SW orientation

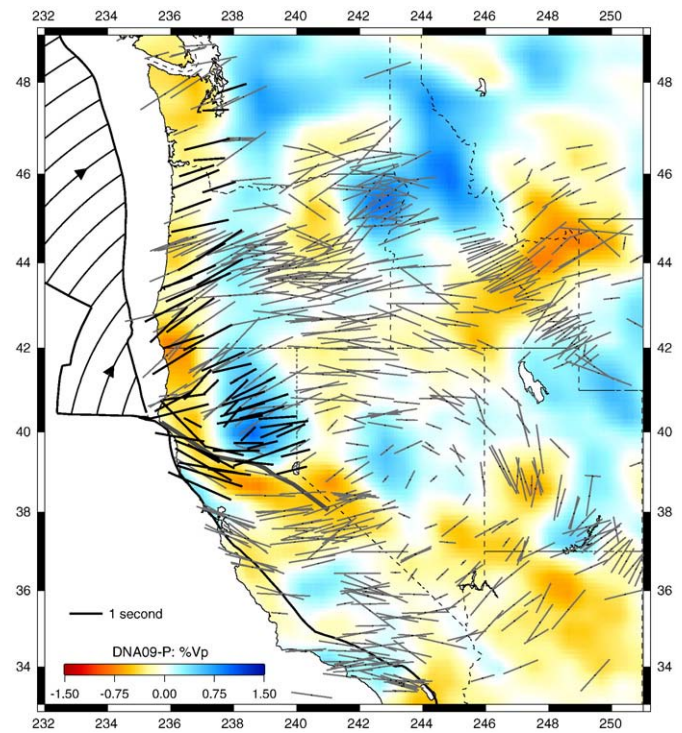


Fig. 2. Regional splitting pattern overlain on the vertically averaged upper mantle velocity anomaly. Our splitting results are shown in black and those of previous studies are in grey (Wang et al., 2008; Zandt and Humphreys, 2008; Long et al., 2009; West et al., 2009 and references therein). The splitting pattern is shown to be uniform trench-normal throughout Cascadia. The velocity anomaly shown is a vertical average of the velocity anomaly from the DNA09 P-wave model over the 100–400 km depth range (Obrebski et al., in press; <http://dna.berkeley.edu>). The slab is imaged as the north–south high velocity feature. The splitting measurements rotate around the southern end of the slab. Curved black lines on the G-JdF plate represent the direction of its absolute plate motion.

further to the east corresponds to the low velocity region that wraps around the southern end of the slab.

Our results are consistent with those of previous studies in the wider region (Fig. 2). To the north and east the splitting remains sub-parallel to the subduction of the G-JdF plate. The rotation of the fast direction immediately south of the slab extends further south throughout the low velocity anomaly of the “slab gap” window in central California. Our study provides improved detail of the regional splitting pattern along Cascadia and especially in Northern California, where there is a rapid switch in fast direction near the triple junction. In Fig. 3 the same tomography image is compared to the delay time of each of the splitting measurements as represented by the size of the circle. We focus on the area over which we have dense measurements. It is notable that there is a correlation between the amplitude of the delay time and the location of high and low velocity anomalies. The splitting delays are lower (small circles) over the strong high velocity (blue) slab signal and similar in magnitude to those over the high velocity feature in central Nevada. In the low velocity regions (orange) surrounding the slab larger delay times (larger circles) are observed.

4. Sources of anisotropy and mantle flow

Determining the primary source of anisotropy can be difficult, especially in subduction zones where there are four distinct possible source regions: the overlying continental lithosphere, the mantle wedge, the slab itself and the sub-slab mantle. The range of back azimuthal coverage available is restricted due to the temporary nature of the network deployments. Therefore we cannot make a reliable

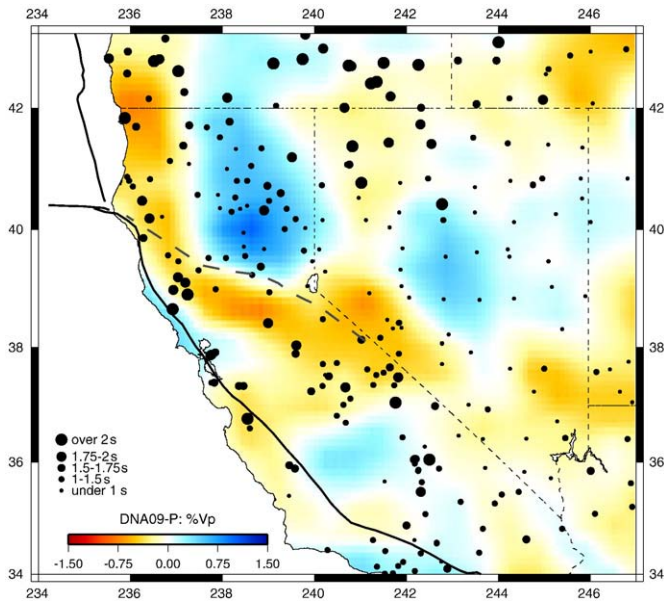


Fig. 3. Spatial variation of delay time. Splitting measurements are plotted as black circles with radius proportional to the observed delay time at that station. The velocity anomaly image is the same as Fig. 2. Smaller delay times are generally seen over high velocity anomalies (blue) and larger delay times over low velocity areas (orange).

assessment of any fast direction variations with back azimuth, if they should exist, which would allow for investigation of layered anisotropy and dipping axes. We can say that the fast direction remained constant for the reasonable range of back azimuths that were contained in the event catalog, especially for the FACES stations for which we had data over a longer time period (see rose diagrams in [Supplementary material](#)).

The previous study of northern Cascadia by [Currie et al. \(2004\)](#) was able to characterize 2 layers of anisotropy over the North American craton (a combination of anisotropy from the thick continental lithosphere and from the mantle below) but did not find any back azimuthal variation over the Cascadia subduction zone. The shallow dip of the slab in this region ($<30^\circ$), and therefore also any anisotropy, was not expected to cause a significant variation in the splitting parameters. The study of southern Cascadia by [Hartog and Schwartz \(2000\)](#) did find an azimuthal variation, which they modeled as anisotropy dipping $\sim 50^\circ$ towards the northeast, consistent with subduction in the region. The uniformity of the splitting observations between our closely spaced stations and over a wide geographic area, the entire length and breadth of Cascadia, suggests simple anisotropy i.e. a single layer. Multiple layers could also be present if the splitting direction is the same for both. For example it is quite possible that both the slab and sub-slab mantle could have the same alignment, if the underlying mantle flow is driven by nearby subduction and its orientation is ‘frozen in’ to the base of the newly forming G-JdF lithosphere at the ridge. In this section we consider the arguments for and against each of the possible source regions in Cascadia.

Given the size of the observed delay times (average >1 s) it is highly unlikely that the primary source could be from the continental lithosphere. Previous shear wave splitting studies suggest that contributions from continents are often small and insignificant compared to the mantle ([Özalaybey and Savage, 1995](#); [Silver, 1996](#); [Currie et al., 2004](#)). In addition the lithosphere of the western US is known for being thin ([Li et al., 2007](#)). Neither is the fast direction aligned with the tectonic fabric of the lithosphere nor any crustal features. We therefore expect the splitting contribution from the continental lithosphere to be negligible compared to mantle sources,

in accordance with other studies of the western US (e.g. [Silver and Holt, 2002](#)).

Anisotropy of the mantle wedge is usually determined by analyzing local S waves from the subduction zone. This has not been possible for Cascadia due to the abnormal lack of seismicity in this region. It is possible that stations located in the backarc, i.e. easterly Mendocino stations, where the wedge thickness is in the order of 100–150 km ([Obrebski et al., in press](#)) could have a primary contribution from this region, and the average delay time is of an appropriate magnitude (~ 1.2 s). The fast direction is consistent with the G-JdF to North America relative plate motion and also the absolute motion of the North American plate as would be expected for shearing of the mantle wedge and corner flow. However for the Mendocino and FACES stations located along the west coast there is zero wedge thickness, so there cannot be any contribution from the wedge. The splitting pattern is uniform over the forearc and backarc ([Fig. 2](#)) suggesting that the primary source region is the same for both. We do not observe an increase in delay time from west to east ([Fig. 3](#)) as might also be expected due to an increasing wedge thickness if anisotropy from the wedge was providing a large contribution to the splitting signal. At some point to the east there must be a complete transition to the continental-side mantle as we move past the subduction zone. This may occur around the California–Nevada boundary where the wedge is approaching several hundred kilometer thickness ([Obrebski et al., in press](#)), which constitutes the generally accepted lower boundary of anisotropic material and where we do observe a change in the fast direction from uniform NE–SW consistent with subduction to a more E–W orientation in the east.

The subducting G-JdF plate is young (7–10 Ma at the trench) ([Severinghaus and Atwater, 1990](#); [Wilson, 1993](#)) and based on this age the lithosphere is expected to be less than 50 km thick ([Fowler, 1990](#)). Based on tomography the slab has an approximate dip of 50° ([Roth et al., 2008](#); [Obrebski et al., in press](#)). By taking into account the thickness, dip of the slab, and inclination of incoming SKS and SKKS waves ($<10^\circ$ from the vertical), the predicted path length through the dipping slab is $80 \text{ km} \pm 15 \text{ km}$. This equates to an approximate delay time of $0.7 \text{ s} \pm 0.1 \text{ s}$ ([Silver and Chan, 1988](#)) assuming 4% anisotropy ([Christensen and Lundquist, 1982](#)) and an S-wave velocity of 4.6 km/s ([Grand and Helmlinger, 1984](#)). It therefore seems unlikely that all of the splitting delay is generated within the slab given the size of the delay times observed, although we cannot rule out a contribution from the slab.

In addition, the fast direction shows no correlation with the spreading direction or orientation of the ridge as is expected for fossil anisotropy of an oceanic plate ([Peyton et al., 2001](#)). Recently there have been studies relating the splitting patterns of global subduction zones to hydrated faults within the subducting plate ([Faccenda et al., 2008](#); [Healy et al., 2009](#)). Although the deformation of the Juan de Fuca and Gorda plates has produced some NE–SW trending left lateral faults ([Wilson, 1988, 1989](#); [Chaytor et al., 2009](#)) that are sub-parallel to the observed fast direction, the main anisotropic source for Cascadia is not expected to come from an internal deformation of the slab. This is because the G-JdF slab is young and thin restricting slab hydration to shallow depths and limiting the thickness of the anisotropic layer ([Faccenda et al., 2008](#)).

By process of elimination we are left with the sub-slab mantle as the most likely source region of anisotropy. It is the only region that is large enough (>200 km) to produce up to 2 s delay time ([Silver and Chan, 1988](#)) as observed on the west coast of Oregon and is also capable of producing the consistent splitting orientation throughout the subduction zone. As the fast direction is parallel to subduction of the G-JdF plate this is consistent with entrained mantle flow beneath the slab being the source of the anisotropy. This interpretation is also consistent with that of previous shear wave splitting studies in the region ([Hartog and Schwartz, 2000](#); [Currie et al., 2004](#)). Alternatively the mantle beneath the slab could be flowing in the opposite direction

induced by the rollback of the Gorda slab. Laboratory and numerical models of a slab rollback predict a toroidal flow pattern (Kincaid and Griffiths, 2003; Funicello et al., 2006; Piromallo et al., 2006). As the trench retreats mantle material from below is forced oceanward and then around the edge of the slab into the mantle wedge which is under lower pressure.

Immediately south of the MTJ there is a dramatic change in the splitting direction from NE–SW along Cascadia to NW–SE south of the MTJ. In addition there is a gradual rotation of the splitting observation south of the MTJ from west to east. The splits rotate from NW–SE at the coast to NE–SW beneath northeastern California (Fig. 1). Fig. 2 shows the relationship between this splitting rotation and the southern edge of the Gorda slab suggesting that the anisotropy is due to flow around the southern edge of the slab. Peyton et al. (2001) provide another documented case in Kamchatka of flow around a slab edge as determined from shear wave splitting. They too observed a dramatic change in fast direction over a short distance. However the relative orientation of splitting is reversed as the fast direction is trench-parallel over the subducting plate in Kamchatka, whereas it is trench-normal in Cascadia.

Overall we consider the observed pattern of anisotropy to be best explained by entrained mantle flow due to the consistency with the subduction direction. This entrained mantle flow then appears to be modified by and diverted around the southern edge of the Gorda slab instead following a purely toroidal flow pattern. Our preferred interpretation is illustrated in Fig. 4. In this case the anisotropy is thought to have a dipping axis. In order to confirm the presence of dipping anisotropy a wide range of back azimuths is required and is therefore impossible to investigate with temporary seismic networks such as ours. Previous studies utilizing data from permanent stations in the Pacific Northwest have however been able to perform such analyses, the results of which also led them to infer entrained mantle flow as mentioned previously (Hartog and Schwartz, 2000; Currie et al., 2004). Even with permanent stations detailed forward modeling is required and constraining dip remains extremely difficult and non-unique (Chevrot and van der Hilst, 2003). Significant variations in splitting parameters with back azimuth only occur when the dip is more than 30° (Savage, 1999; Chevrot, 2000). Even then the fast direction observed will remain parallel or sub-parallel to the orientation of the fast axis and only the delay time will vary greatly (Savage, 1999; Marson-Pidgeon and Savage, 2004). A good match to the delay time can always be found by simply changing the path length (Hartog and Schwartz, 2000). As we do not know the thickness of the anisotropic layer it is therefore very difficult to constrain the dip.

Even though Hartog and Schwartz (2000) achieved an improvement in fit when allowing for dipping axes and the subsequent results were very much consistent with subduction in Cascadia their uncertainty in dip remains in the order of 30° or more. We therefore refrain from making assertions on the precise dip of anisotropy but we can say that for a fast axis with the same orientation as the inclined slab we would expect fast

directions similar to what we observe i.e. predominantly trench-normal (Russo and Silver, 1994).

Previously, flow around a slab has been inferred to account for trench-parallel splitting, as the mantle tries to move around a slab that is undergoing rollback (Russo and Silver, 1994; Peyton et al., 2001; Anderson et al., 2004). This study has produced evidence for flow around the slab edge but without trench-parallel flow beneath the subducting plate. This is unique to Cascadia where the effect of rollback on the mantle flow field only appears to be at the slab edge.

A barrier to mantle flow at depth is often inferred to explain trench-parallel flow beneath slabs in subduction zones (Russo and Silver, 1994; Long and Silver, 2009). Either such a barrier is not present in Cascadia implying the possibility of entrainment of mantle material through the transition zone along with the sinking slab, or the base of the slab is shallow, potentially due to a tear in the slab from interaction with the Yellowstone plume (Xue and Allen, 2007; Obrebski et al., in press) allowing for return flow underneath the bottom of the slab. Laboratory models of rollback during subduction have predicted the possibility of such return flow (Kincaid and Griffiths, 2003). The latest tomography models show the G-JdF slab to be especially shallow beneath Oregon, only extending to 300 km depth (Obrebski et al., in press). As such the slab isn't long enough to provide a substantial barrier to mantle flow. Instead it would be possible for the mantle to migrate eastward beneath the plate margin. A hole in the slab could therefore explain why Cascadia is the only subduction zone to display consistently trench-normal splitting in the sub-slab mantle.

Fig. 2 shows the regional pattern of splitting for the entire western US. The large-scale circular pattern centered upon Nevada (the “Nevada swirl”) was first identified by Savage and Sheehan (2000) and was later modeled as toroidal flow around the G-JdF slab (Zandt and Humphreys, 2008). More recently West et al. (2009) have interpreted a high velocity anomaly beneath central Nevada (see Fig. 2) as a lithospheric drip that could also explain the same circular pattern of splits. In our study of the splitting observations in northern California we interpret the anisotropy as indicative of flow around the southern edge of the Gorda slab but on a smaller scale than previously proposed by Zandt and Humphreys (2008). From the regional splitting pattern in Fig. 2 we can see that the slab-edge rotation continues throughout central California but is directed towards the center of the Nevada high velocity anomaly, i.e. the center of the “Nevada swirl.” The improved level of detail provided by our results to the regional splitting pattern, especially in northern California, therefore gives better geographical constraints on these previously proposed flow geometries. We are now able to distinguish that flow around the slab edge is a separate feature from anisotropy associated with the Nevada anomaly.

5. Conclusion

Immediately south of the MTJ, shear wave splitting observations are observed to rotate from NW–SE at the coast to NE–SW beneath northeastern California. This rotation of the seismic anisotropy fast directions is aligned with the southern edge of the G-JdF plate as imaged tomographically and is therefore strongly indicative of flow around the edge of the slab. This appears to be distinct from and possibly separate to the larger-scale circular pattern of anisotropy centered on a high velocity anomaly beneath central Nevada (West et al., 2009). To the north, a uniform splitting pattern that is trench-normal is observed throughout Cascadia, consistent with entrained mantle flow beneath the subducted slab that is unique to the global shear wave splitting data set (Long and Silver, 2008; Long and Silver, 2009). In most other subduction zones a barrier to mantle flow at depth i.e. the transition zone, is inferred to explain trench-parallel flow of mantle material beneath subducting slabs (Long and Silver, 2009). In the case of Cascadia, the mantle flow is entrained with the slab moving downwards towards the transition zone.

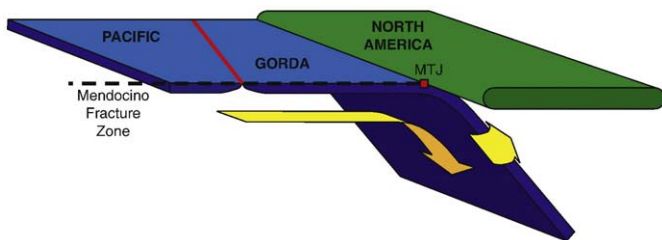


Fig. 4. Schematic diagram of inferred mantle flow in the Cascadia subduction zone. Sub-slab mantle is entrained beneath the slab generating subduction-parallel, trench-normal fast splitting observations. Flow around the southern end of the slab generates the rotation of fast directions in the region of the MTJ.

This suggests either no barrier to mantle flow at depth, or a shallow bottom to the slab allowing flow beneath the slab-bottom.

Acknowledgments

This work was funded by awards EAR-0643392, EAR-0745934 and EAR-0643077 from the National Science Foundation's Earthscope program. We extend our thanks to Andreas Wüstfeld for providing guidance concerning SplitLab, and to Gene Humphreys, Maureen Long, John West and George Zandt for sharing their shear wave splitting data sets. Improvements to the manuscript were made possible thanks to helpful suggestions from an anonymous reviewer. The figures were produced using GMT (Wessel and Smith, 1991) and IRIS DMC provided the seismic data.

Appendix A. Supplementary data

Supplementary data associated with this article can be found, in the online version, at doi:10.1016/j.epsl.2010.07.015.

References

- Anderson, M.L., Zandt, G., Triep, E., Fouch, M., Beck, S., 2004. Anisotropy and mantle flow in the Chile–Argentina subduction zone from shear wave splitting analysis. *Geophys. Res. Lett.* 31. doi:10.1029/2004GL020906.
- Ando, M., Ishikawa, Y., Yamazaki, F., 1983. Shear wave polarization anisotropy in the upper mantle beneath Honshu, Japan. *J. Geophys. Res.* 88, 5850–5864.
- Barruol, G., Silver, P.G., Vauchez, A., 1997. Seismic anisotropy in the eastern US: deep structure of a complex continental plate. *J. Geophys. Res.* 102, 8329–8348.
- Bostock, M.G., Cassidy, J.F., 1995. Variations in SKS splitting across western Canada. *Geophys. Res. Lett.* 22, 5–8.
- Bowman, J.R., Ando, M., 1987. Shear wave splitting in the upper-mantle wedge above the Tonga subduction zone. *Geophys. J. R. Astron. Soc.* 88, 25–41.
- Chaytor, J.D., Goldfinger, C., Dziak, R.P., Fox, C.G., 2009. Active deformation of the Gorda plate: constraining deformation models with new geophysical data. *Geology* 32, 353–356.
- Chevrot, S., 2000. Multichannel analysis of shear wave splitting. *J. Geophys. Res.* 105, 21,579–21,590.
- Chevrot, S., van der Hilst, R., 2003. On the effects of a dipping axis of symmetry on shear wave splitting measurements in a transversely isotropic medium. *Geophys. J. Int.* 152, 497–505.
- Christensen, N.I., Lundquist, S.M., 1982. Pyroxene orientation within the upper mantle. *Geol. Soc. Am. Bull.* 93, 279–288.
- Currie, C.A., Cassidy, J.F., Hyndman, R.D., Bostock, M.G., 2004. Shear wave anisotropy beneath the Cascadia subduction zone and western North America craton. *Geophys. J. Int.* 157, 341–353.
- Fabritius, R.A., 1995. Shear-wave Anisotropy across the Cascadia Subduction Zone from a Linear Seismograph Array. Oregon State University, M.S.
- Faccenna, M., Burlini, L., Gerya, T.V., Mainprice, D., 2008. Fault-induced seismic anisotropy by hydration in subducting oceanic plates. *Nature* 455, 1097–1101.
- Fouch, M.J., Fischer, K.M., 1996. Mantle anisotropy beneath northwest Pacific subduction zones. *J. Geophys. Res.* 101 (B7), 15,987–16,002.
- Fowler, C.M.B., 1990. *The Solid Earth: An Introduction to Global Geophysics*. Cambridge University Press, Cambridge, England.
- Funiciello, F., Moroni, M., Piromallo, C., Faccenna, C., Cenedese, A., Bui, H.A., 2006. Mapping mantle flow during retreating subduction: laboratory models analyzed by feature tracking. *J. Geophys. Res.* 111, B03402. doi:10.1029/2005JB003792.
- Gaherty, G.B., Jordan, T.H., 1995. Lehmann discontinuity as the base of an anisotropic layer beneath continents. *Science* 268, 1468–1471.
- Grand, S., Helmberger, D., 1984. Upper mantle shear structure of North America. *Geophys. J. R. astr. Soc.* 76, 399–438.
- Gripp, A.E., Gordon, R.G., 2002. Young tracks of hotspots and current plate velocities. *Geophys. J. Int.* 150, 321–361. doi:10.1046/j.1365-246X.2002.01627.x.
- Hartog, R., Schwartz, S.Y., 2000. Subduction-induced strain in the upper mantle east of the Mendocino triple junction, California. *J. Geophys. Res.* 105, 7909–7930.
- Healy, D., Reddy, R.M., Timms, N.E., Gray, E.M., Brovarone, A.V., 2009. Trench-parallel fast axes of seismic anisotropy due to fluid-filled cracks in subducting slabs. *Earth Planet. Sci. Lett.* 283, 75–86.
- Kincaid, C., Griffiths, R.W., 2003. Laboratory models of the thermal evolution of the mantle during rollback subduction. *Nature* 425, 58–62.
- Li, X.Q., Yuan, X.H., Kind, R., 2007. The lithosphere–asthenosphere boundary beneath the western United States. *Geophys. J. Int.* 170, 700–710.
- Long, M.D., Silver, P.G., 2008. The subduction zone flow field from seismic anisotropy: a global view. *Science* 319, 315–318.
- Long, M.D., Silver, P.G., 2009. Mantle flow in subduction systems: 1. The sub-slab flow field and implications for mantle dynamics. *Journal of Geophysical Research*.
- Long, M.D., van der Hilst, R.D., 2005. Upper mantle anisotropy beneath Japan from shear wave splitting. *Phys. Earth Planet. Inter.* 151, 206–222.
- Long, M.D., Gao, H., Klaus, A., Wagner, L.S., Fouch, M.J., James, D.E., Humphreys, E., 2009. Shear wave splitting and the pattern of mantle flow beneath eastern Oregon. *Earth Planet. Sci. Lett.* 288, 359–369.
- Marson-Pidgeon, K., Savage, M.K., 2004. Modeling shear wave splitting observations from Wellington, New Zealand. *Geophys. J. Int.* 157, 853–864.
- Nakajima, J., Hasegawa, A., 2004. Shear-wave polarization anisotropy and subduction-induced flow in the mantle wedge of northern Japan. *Earth Planet. Sci. Lett.* 225, 365–377.
- Obrebski, M., Allen, R.M., Xue, M., Hung, S-H., in press. Slab–plume interaction beneath the Pacific Northwest. *Geophys. Res. Lett.*
- Özalaybey, S., Savage, M., 1995. Shear-wave splitting beneath western United States in relation to plate tectonics. *J. Geophys. Res.* 100, 18,135–18,149.
- Peyton, V., Levin, V., Park, J., Brandon, M., Lees, J., Gordeev, E., Ozerov, A., 2001. Mantle flow at a slab edge: seismic anisotropy in the Kamchatka region. *Geophys. Res. Lett.* 28, 379–382.
- Piromallo, C., Becker, T.W., Funiciello, F., Faccenna, C., 2006. Three-dimensional instantaneous mantle flow induced by subduction. *Geophys. Res. Lett.* 33, L08304. doi:10.1029/2005GL025390.
- Polet, J., Kanamori, H., 2002. Anisotropy beneath California; shear wave splitting measurements using a dense broadband array. *Geophys. J. Int.* 149, 313–317. doi:10.1046/j.1365-246X.2002.01630.x.
- Roth, J.B., Fouch, M.J., James, D.E., Carlson, R.W., 2008. Three-dimensional seismic velocity structure of the northwestern United States. *Geophys. Res. Lett.* 35, L15304. doi:10.1029/2008GL034669.
- Russo, R.M., Silver, P.G., 1994. Trench-parallel flow beneath the Nazca plate from seismic anisotropy. *Science* 263, 1105–1111.
- Sandvol, E., Ni, J., 1997. Deep azimuthal seismic anisotropy in the southern Kurile and Japan subduction zones. *J. Geophys. Res.* 102, 9911–9922.
- Savage, M.K., 1999. Seismic anisotropy and mantle deformation: what we have learned from shear wave splitting? *Rev. Geophys.* 37, 65–106.
- Savage, M.K., Sheehan, A.F., 2000. Seismic anisotropy and mantle flow from the Great Basin to the Great Plains, western United States. *J. Geophys. Res.* 105, 13,715–13,734. doi:10.1029/2000JB900021.
- Severinghaus, J., Atwater, T., 1990. Cenozoic geometry and thermal state of the subducting slabs beneath North America. In: Wernicke, B.P. (Ed.), *Basin and range extensional tectonics near the latitude of Las Vegas, Nevada: Geological Society of America Memoir*, 176, pp. 1–22.
- Silver, P.G., 1996. Seismic anisotropy beneath the continents: probing the depths of geology. *Annu. Rev. Earth Planet. Sci.* 24, 385–432.
- Silver, P.G., Chan, W.W., 1988. Implications for continental structure and evolution from seismic anisotropy. *Nature* 335, 34–39.
- Silver, P.G., Chan, W.W., 1991. Shear wave splitting and subcontinental mantle deformation. *J. Geophys. Res.* 96, 429–454.
- Silver, P.G., Holt, W.E., 2002. The mantle flow field beneath western North America. *Science* 295, 1054–1057. doi:10.1126/science.1066878.
- Tono, Y., Fukao, Y., Kunugi, T., Tsuboi, S., 2009. Seismic anisotropy of the Pacific slab and mantle wedge beneath the Japanese islands. *J. Geophys. Res.* 114, B07307. doi:10.1029/2009JB006290.
- Wang, X., Ni, J.F., Aster, R., Sandvol, E., Wilson, D., Sine, C., Grand, S.P., Baldrige, W.S., 2008. Shear-wave splitting and mantle flow beneath the Colorado Plateau and its boundary with the Great Basin. *Bull. Seismol. Soc. Am.* 98, 2526–2532.
- Wessel, P., Smith, W.H.F., 1991. Free software helps map and display data. *EOS Trans. AGU* 72 (41), 441.
- West, J.D., Fouch, M.J., Roth, J.B., Elkins-Tanton, L.T., 2009. Vertical mantle flow associated with a lithospheric drip beneath the Great Basin. *Nat. Geosci.* 2, 439–444.
- Wilson, D.S., 1988. Tectonic history of the Juan de Fuca Ridge over the last 40 million years. *J. Geophys. Res.* 93, 11,863–11,876.
- Wilson, D.S., 1989. Deformation of the so-called Gorda Plate. *J. Geophys. Res.* 94, 3065–3075.
- Wilson, D.S., 1993. Confidence intervals for motion and deformation of the Juan de Fuca Plate. *J. Geophys. Res.* 98, 16,053–16,071.
- Wüstfeld, A., Bokelmann, G., 2007. Null detection in shear-wave splitting measurements. *Bull. Seismol. Soc. Am.* 97 (4), 1204–1211.
- Wüstfeld, A., Bokelmann, G., Zaroli, C., Barruol, G., 2007. SplitLab: a shear-wave splitting environment in Matlab. *Comput. Geosci.* 34, 515–528.
- Xue, M., Allen, R.M., 2006. Origin of the Newberry hotspot track: evidence from shear-wave splitting. *Earth Planet. Sci. Lett.* 244, 315–322.
- Xue, M., Allen, R.M., 2007. The fate of the Juan de Fuca plate: implications for a Yellowstone plume head, Earth and planet. *Sci. Lett.* 264, 266–276.
- Zandt, G., Humphreys, E., 2008. Toroidal mantle flow through the western US slab window. *Geology* 36, 295–298.
- Zhang, S., Karato, S.I., 1995. Lattice preferred orientation of olivine aggregates deformed in simple shear. *Nature* 375, 774–777. doi:10.1038/375774a0.

Supplementary Material for:

**Seismic Anisotropy beneath Cascadia and the Mendocino Triple Junction:
Interaction of the Subducting Slab with Mantle Flow**

**Caroline M Eakin^{1,2}, Mathias Obrebski¹, Richard M Allen¹, Devin C Boyarko³ Michael R
Brudzinski³ and Robert Porritt¹**

¹ Dept. Earth & Planetary Sciences, University of California, Berkeley, USA

² Dept. of Earth Science and Engineering, Imperial College London, UK

³ Dept. of Geology, Miami University, Oxford, Ohio 45046, USA

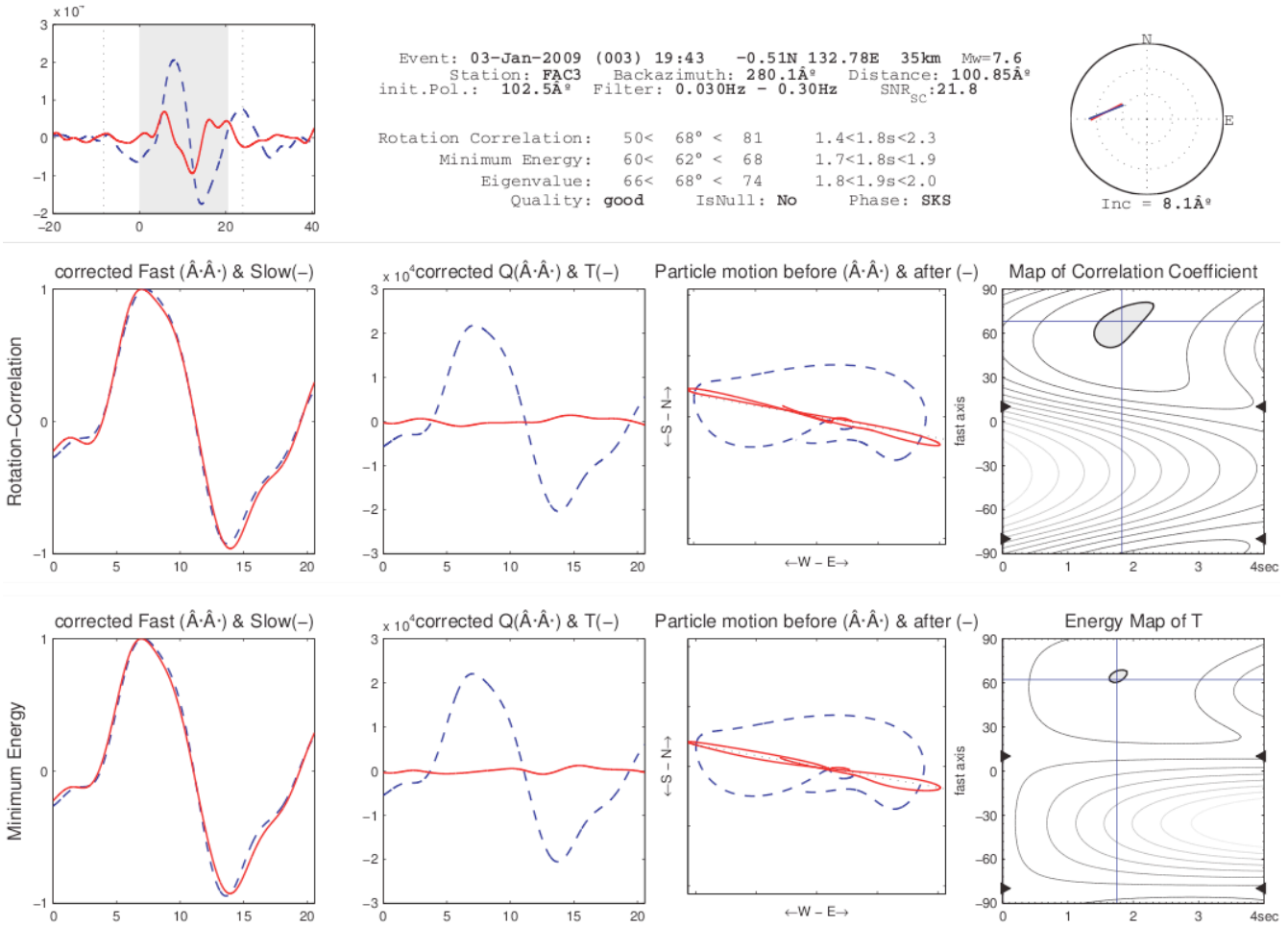


Figure S1. Example of a shear wave splitting calculation from station FAC3 in Oregon performed using SplitLab [Wüstfeld *et al.*, 2007]. The upper left corner shows the uncorrected radial (dashed blue) and transverse (red) components with the selected time window in grey. In the upper right hand corner is a rose diagram of the splitting result calculated by the two methods. The middle row shows splitting diagnostics for the rotation correlation method [Bowman and Ando, 1987] and the lower row is for the minimum energy method [Silver and Chan, 1988, 1991]. The first plot on the left shows how well the arrivals match on each component. The second plot shows the waveforms after they have been corrected for splitting. The third plot shows the initial (blue) and corrected (red) particle motion. The last figure is a contour plot of the error surface, the shaded area of which represents the 95% confidence level.

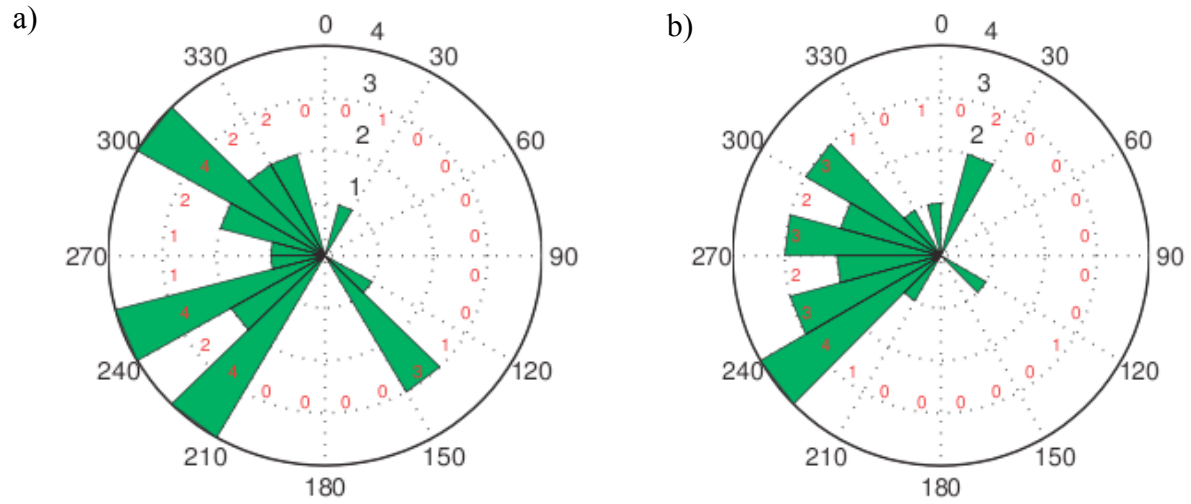
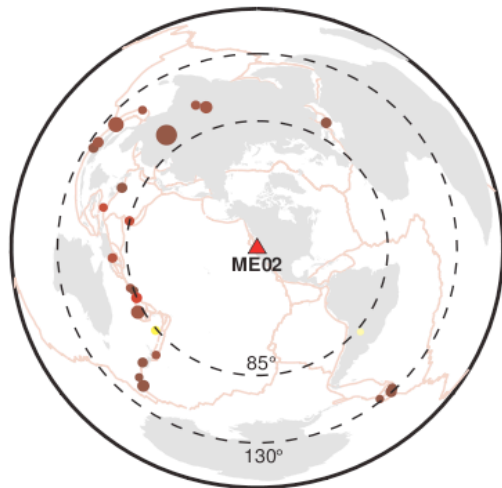


Figure S2. Rose diagrams for (a) the Mendocino Experiment, and (b) FACES network showing the back azimuth distribution of events used in this study. The length of the wedge and the number written in red indicates the number of events in each bin. The back azimuth range is restricted for both networks with suitable events preferentially occurring in the northwest to southwest directions.

a)

Earthquakes in window [85° – 130°] around station ME02
05-Oct-2007 – 11-Sep-2008
 $6.25 \leq M_w \leq 10$
 $0 \leq \text{depth} \leq 1000$



b)

Earthquakes in window [85° – 130°] around station FACG
25-Nov-2007 – 01-Jul-2009
 $6.25 \leq M_w \leq 10$
 $0 \leq \text{depth} \leq 1000$

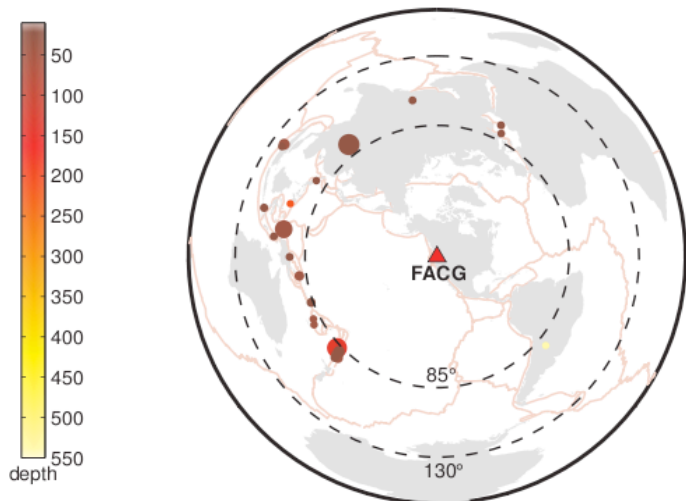


Figure S3. Event location map of for (a) the Mendocino Experiment, and (b) the FACES network showing the distribution of events used in this study. Dashed lines show the epicentral distance range of 85° to 130° from which events were selected. The size of each dot indicates the magnitude of the event and the color indicates its depth. The majority of events which meet our criteria are located in the Indonesian and Tonga subduction zones.

Table S1**(a)** List of events used for the Mendocino network.

Date	Time	Latitude	Longitude	Depth (km)	Mw	Back Azimuth	Epicentral Distance
15/10/07	12:29:37	-44.7°	167.5°	25	6.8	225.0°	106.7°
24/10/07	21:02:51	-3.9°	101.1°	30	6.8	303.2°	128.2°
10/11/07	01:13:34	-52.2°	159.5°	10	6.5	222.0°	115.4°
22/11/07	08:48:31	-5.8°	147.0°	78	6.7	267.3°	95.9°
27/11/07	11:50:01	-11.0°	162.2°	42	6.6	253.6°	87.8°
20/12/07	07:55:19	-38.8°	177.9°	36	6.6	223.8°	97.0°
10/02/08	12:22:03	-60.8°	-25.5°	10	6.5	142.8°	126.3°
14/02/08	10:09:23	36.6°	21.8°	30	6.9	29.8°	95.8°
23/02/08	15:57:20	-57.1°	-23.4°	10	6.7	138.1°	126.1°
25/02/08	08:36:35	-2.4°	100.0°	35	6.9	305.5°	127.6°
25/02/08	21:02:20	-2.2°	99.8°	39	6.5	305.7°	127.6°
03/03/08	14:11:13	13.3°	125.7°	18	6.8	296.0°	99.0°
09/05/08	21:51:31	12.5°	143.2°	88	6.7	283.8°	87.0°
27/06/08	11:40:17	11.0°	91.9°	35	6.6	322.6°	121.0°
30/06/08	06:17:43	-58.2°	-21.9°	10	7.0	139.0°	127.2°
19/07/08	09:27:04	-11.1°	164.5°	30	6.6	252.1°	86.1°
25/08/08	13:22:02	30.9°	83.6°	35	6.7	338.9°	105.7°
08/09/08	18:52:08	-13.5°	167.0°	122	6.9	248.6°	86.0°
11/09/08	00:00:03	1.9°	127.4°	98	6.6	286.3°	105.7°
05/10/07	07:17:53	-25.1°	179.4°	508	6.5	230.5°	85.8°
16/10/07	21:05:41	-25.5°	179.5°	477	6.6	230.2°	86.0°
20/02/08	08:08:31	2.8°	96.0°	34	7.4	312.0°	123.6°
20/03/08	22:33:01	35.4°	81.4°	37	7.1	340.6°	99.9°
09/04/08	12:46:13	-20.1°	168.9°	35	7.3	241.2°	88.5°
12/04/08	00:30:11	-55.7°	158.5°	10	7.1	218.8°	118.0°
12/05/08	06:28:00	31.1°	103.3°	10	7.9	322.0°	96.0°
03/09/08	11:25:13	-26.6°	-63.2°	547	6.3	131.2°	85.1°

(b) List of events used for the FACES network.

Date	Time	Latitude	Longitude	Depth (km)	Mw	Back Azimuth	Epicentral Distance
25/11/07	16:02:17	-8.3°	118.4°	30	6.5	285.8°	115.7°
09/12/07	07:28:20	-25.9°	-177.5°	149	7.8	227.3°	87.5°
15/12/07	09:39:49	-6.7°	131.2°	20	6.4	277.1°	105.9°
25/02/08	08:36:35	-2.4°	100.0°	35	6.9	306.5°	122.4°
09/04/08	11:13:21	-20.2°	168.8°	35	6.3	240.8°	90.7°
12/05/08	06:28:00	31.1°	103.3°	10	7.9	321.9°	92.1°
01/06/08	01:57:22	20.1°	121.3°	22	6.3	302.3°	92.0°
08/06/08	12:25:29	38.0°	21.5°	10	6.3	27.4°	89.8°
19/07/08	09:27:04	-11.1°	164.5°	30	6.6	249.9°	86.4°
03/09/08	11:25:13	-26.6°	-63.2°	547	6.3	129.5°	90.6°
29/09/08	15:19:31	-29.9°	-177.7°	35	7.0	225.2°	90.9°
28/10/08	23:09:58	30.6°	67.3°	15	6.4	351.1°	102.5°
09/12/08	06:24:02	-31.1°	-177.0°	35	6.7	224.1°	91.6°
25/12/08	03:20:29	5.8°	125.5°	208	6.3	289.9°	100.4°
03/01/09	19:43:54	-0.5°	132.8°	35	7.6	280.2°	100.3°
03/01/09	22:33:42	-0.7°	133.3°	35	7.4	279.7°	100.1°
18/02/09	21:53:45	-27.4°	-176.4°	25	6.9	225.7°	88.3°
01/04/09	03:55:02	-3.6°	143.9°	10	6.4	269.9°	94.9°
15/04/09	20:01:33	-3.1°	100.5°	8	6.4	305.5°	122.7°
16/05/09	00:53:46	-31.5°	-178.9°	10	6.5	225.1°	92.9°
02/06/09	02:17:07	-17.8°	167.9°	40	6.3	243.0°	89.4°
23/06/09	14:19:16	-5.3°	153.4°	35	6.7	261.9°	89.6°
01/07/09	09:30:09	34.2°	25.5°	10	6.4	25.9°	94.5°

Table S2

List of stacked splitting measurements at Mendocino and FACES stations.

Station	Latitude (°)	Longitude (°)	Φ (°)	δt (s)
ME02	41.7	-122.3	66	1.40
ME03	41.7	-123.9	58	1.55
ME05	41.5	-122.1	77	1.20
ME06	41.3	-121.7	61	0.90
ME08	40.2	-123.3	-62	0.60
ME09	41.1	-122.7	46	0.60
ME11	41.1	-121.4	64	1.45
ME14	41.0	-121.9	46	0.90
ME15	40.8	-121.7	72	1.35
ME16	40.6	-122.1	44	0.65
ME17	40.5	-121.7	73	1.40
ME18	40.7	-121.0	72	1.50
ME20	40.5	-121.0	72	1.15
ME23	40.4	-121.5	76	0.70
ME24	40.4	-122.0	40	0.80
ME25	40.3	-121.8	80	1.40
ME29	41.1	-123.1	42	1.20
ME30	40.8	-123.6	82	1.30
ME31	40.7	-123.9	62	1.20
ME35	40.5	-123.7	76	1.96
ME39	40.2	-123.6	-44	1.95
ME43	39.6	-123.2	-68	1.45
ME45	39.5	-123.0	-60	1.10
ME46	39.2	-123.0	-60	1.95
ME47	39.1	-122.8	-80	1.80
ME48	38.9	-122.8	-72	2.05
ME49	39.9	-123.7	-80	1.50
ME55	38.7	-123.1	-66	2.05
ME60	39.9	-121.5	46	0.60
ME61	39.5	-122.3	-77	1.20
ME62	39.5	-121.9	-90	1.40

ME63	39.3	-122.5	-62	1.15
ME65	39.0	-122.1	-82	1.30
ME80	40.3	-120.6	86	1.15
ME82	39.7	-121.5	90	0.90
ME83	40.2	-120.4	82	1.45
ME84	40.0	-120.2	66	0.95
ME85	40.0	-120.6	68	1.05
ME87	39.7	-121.1	76	0.95
ME88	39.2	-121.3	-84	1.15
ME89	39.4	-121.2	71	1.70
ME91	39.7	-120.2	70	1.00
ME92	39.5	-120.0	76	0.90
ME93	39.1	-120.2	76	0.95
FAC3	44.4	-122.5	56	1.65
FACA	47.9	-122.1	72	0.95
FACC	47.4	-122.6	88	0.80
FACD	46.7	-122.9	76	1.40
FACF	46.3	-122.8	86	0.95
FACG	46.1	-123.2	72	1.10
FACH	45.9	-123.2	68	1.55
FACI	45.7	-122.5	72	1.05
FACJ	45.3	-123.3	70	1.15
FACK	44.8	-123.1	78	1.75
FACL	44.1	-123.0	60	1.65
FACM	43.8	-122.4	60	1.60
FACN	43.7	-123.3	66	1.60
FACO	43.5	-123.8	71	1.00
FACQ	42.9	-124.1	63	1.60
FACR	43.4	-123.1	66	2.15
FACS	42.8	-123.4	54	1.75
FACT	42.6	-124.1	46	1.55
FACU	42.3	-122.8	62	1.65
FACV	42.2	-123.6	72	1.30